Angle-resolved photoemission study of the electronic structure of the quantum spin liquid $EtMe_3Sb[Pd(dmit)_2]_2$

Q. Q. Ge,[1] H. C. Xu,[1] X. P. Shen,[1] M. Xia,[1] B. P. Xie,[1] F. Chen,[1] Y. Zhang,[1] R. Kato,[2] T. Tsumuraya,[2,3] T. Miyazaki,[3] M. Matsunami,[4] S. Kimura,[4] and D. L. Feng[1,*]

[1]*State Key Laboratory of Surface Physics, Department of Physics, and Advanced Materials Laboratory, Fudan University, Shanghai 200433, People's Republic of China*

[2]*Condensed Molecular Materials Laboratory, RIKEN, Wako-shi, Saitama 351-0198, Japan*

[3]*Computational Materials Science Unit, National Institute for Materials Science, Tsukuba, Ibaraki 305-0047, Japan*

[4]*UVSOR Facility, Institute for Molecular Science and the Graduate University for Advanced Studies, Okazaki 444-8585, Japan*

(Received 2 March 2013; revised manuscript received 18 January 2014; published 5 February 2014)

The electronic structure of a quantum spin liquid compound, $EtMe_3Sb[Pd(dmit)_2]_2$, has been studied with angle-resolved photoemission spectroscopy, together with two other $Pd(dmit)_2$ salts in the valence bond solid or antiferromagnetic state. $EtMe_3Sb[Pd(dmit)_2]_2$, being a Mott insulator, has its lower Hubbard band identified, with a soft energy gap at the chemical potential. In addition, the spectral features exhibit anomalously broad linewidth and negligible dispersion, which fit well to the calculated energy levels of an isolated $[Pd(dmit)_2]_2$ dimer. We suggest that these electronic characteristics might be the manifestation of the spin-charge separation in a two-dimensional quantum spin liquid.

DOI: 10.1103/PhysRevB.89.075105 PACS number(s): 71.36.+c, 71.20.Rv, 79.60.Fr

I. INTRODUCTION

A quantum spin liquid (QSL) is an exotic state of matter that has profound implications for magnetism and high-temperature superconductivity [1]. For two-dimensional (2D) spin-1/2 systems in the presence of antiferromagnetic (AFM) interactions, a QSL might be realized if the geometrical frustration is so strong that it completely destroys the long-range magnetic order even at zero temperature, giving rise to a large degeneracy of the ground states. Although the QSL state on a 2D triangular lattice was first proposed in 1973 [2], it is hard to achieve experimentally because the finite three-dimensional magnetic interactions often drive the system into certain ordered states. Recently, some promising QSL candidates were reported [3–11], for example, κ-(BEDT-TTF)$_2$Cu$_2$(CN)$_3$ [3] and $EtMe_3Sb[Pd(dmit)_2]_2$ [4] on 2D triangular lattices, $BaCu_3V_2O_8(OH)_2$ [7] on a kagome lattice, and $Na_4Ir_3O_8$ [8] on a hyperkagome lattice. They all show no sign of long-range order down to very low temperatures.

$EtMe_3Sb[Pd(dmit)_2]_2$ (where dmit=1,3-dithiole-2-thione-4,5-dithiolate, Me = CH_3, and Et = C_2H_5), as shown in Fig. 1(a), provides a physical realization of a frustrated spin-1/2 QSL system on a triangular lattice [Fig. 1(b)] [4,12,13]. In fact, a series of layered organic salts $X[Pd(dmit)_2]_2$ are Mott insulators at ambient pressure [14], where X is a nonmagnetic monovalent cation such as Et_2Me_2P, $EtMe_3Sb$, $EtMe_3P$, etc. The recent first-principles calculations have shown that the choice of X would affect the hopping integrals (t, t'), and the strength of the frustration (J'/J) [15,16], where the exchange interaction terms $J' = J_r$ and $J = J_B \simeq J_S$ [Fig. 1(b)]. However, the effective on-site Coulomb interaction (U) is weakly dependent on the choice of X [14]. The different parameters would then give different ground states [15,16]. For example, besides the QSL, $Et_2Me_2P[Pd(dmit)_2]_2$ exhibits AFM order below ~20 K [17], $EtMe_3P[Pd(dmit)_2]_2$ is a valence bond solid (VBS), where two neighboring sites form a spin singlet without magnetic order [18], and $Et_2Me_2Sb[Pd(dmit)_2]_2$ is in a charge-ordered state [19].

The band calculations give a half-filled conduction band for all the QSL, VBS, and AFM $Pd(dmit)_2$ salts [15,16,20,21], but they are Mott insulators due to strong correlations. It has been argued that by reducing U/t, the system goes from a long-range magnetic ordered phase to a QSL, and then to a metallic phase [22]. That is, the QSL state is on the verge of metal-insulator transition [22–24]. More specifically, for the $EtMe_3Sb[Pd(dmit)_2]_2$, its t was estimated to be ~30–55 meV [15,16,21], and U has been estimated to be about 0.7 eV [21]. However, experimentally, little is known on the basic electronic structure of a QSL, such as its band structure and Mott gap.

In this paper, we report the detailed electronic structure of $EtMe_3Sb[Pd(dmit)_2]_2$ measured with angle-resolved photoemission spectroscopy (ARPES). We find three broad spectral features with negligible dispersion within the first 1.5-eV binding energy range, which match well with the calculated energy levels of the isolated dimer based on density-functional theory (DFT) [25]. The broad line shape resembles those of polaronic systems; however, the centroid of the incoherent spectrum does not follow the bare dispersion generated by the band theory as in typical polaronic systems. Moreover, the feature near the chemical potential (μ) is recognized as the lower Hubbard band (LHB), and the Mott gap is a soft one. These anomalous behaviors are different from those of the usual Mott insulators, and we suggest that they might be a direct consequence of the spin-charge separation. Furthermore, we found that the VBS and AFM $Pd(dmit)_2$ salts behave similarly in their nonmagnetic states as the QSL compound.

II. EXPERIMENT

The single crystal of $EtMe_3Sb[Pd(dmit)_2]_2$ is usually a hexagonal piece with typical size of 0.6 × 0.6 × 0.05 mm^3 as

*dlfeng@fudan.edu.cn

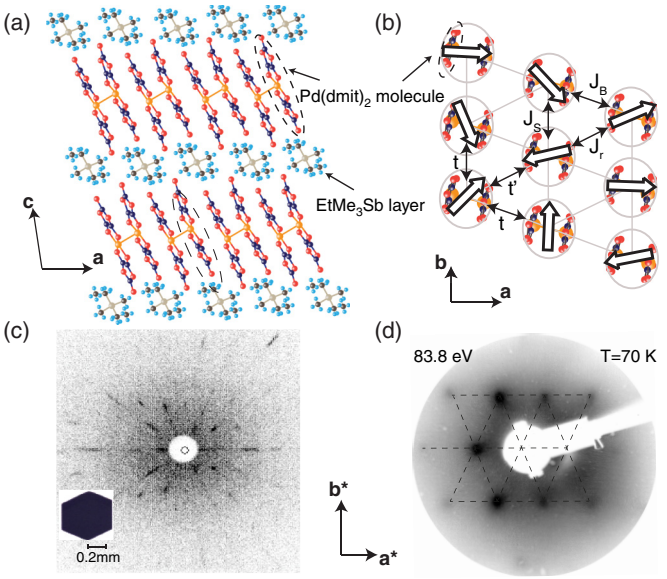

FIG. 1. (Color online) The structure aspects of $EtMe_3Sb[Pd(dmit)_2]_2$. (a) A view from the **b** axis. The crystal structure consists of two-dimensional $Pd(dmit)_2$ layers separated by layers of cation $EtMe_3Sb$. (b) An in-plane sketch of the spin arrangement on the $Pd(dmit)_2$ layer. Each lattice (encircled by solid lines) stands for a strongly dimerized $[Pd(dmit)_2]_2^-$ unit with spin-1/2. Three nearest-neighbor exchange interactions, J_B, J_S, and J_r, are similar and estimated to be 220–250 K. (c) The Laue picture of the $EtMe_3Sb[Pd(dmit)_2]_2$ single crystal. Because the dimer units in (a) stack along the $\mathbf{a}+\mathbf{b}$ direction in one layer and along the $\mathbf{a}-\mathbf{b}$ direction in the next layer [14], the crystal shows twofold symmetry. The inset shows the photo of a single crystal. (d) The low-energy electron diffraction pattern. The dashed lines are a guide for the eye, and we note that the pattern is slightly distorted at the edge.

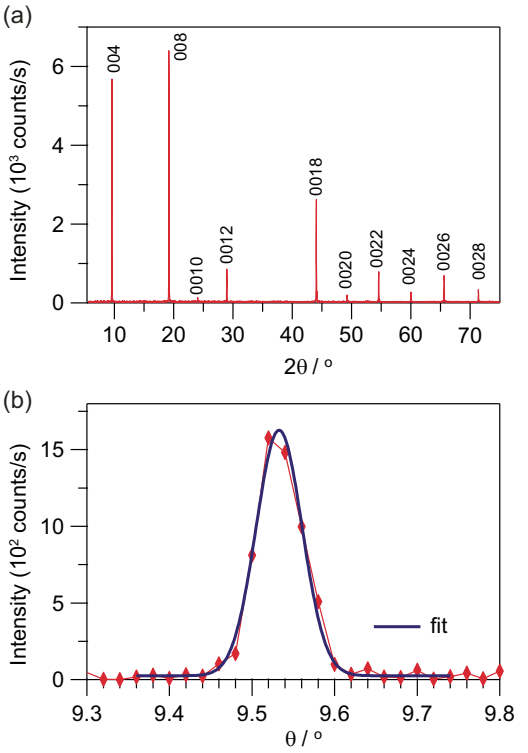

FIG. 2. (Color online) (a) The x-ray diffraction data of an $EtMe_3Sb[Pd(dmit)_2]_2$ single crystal. (b) The rocking curve of the (008) Bragg peak, which is fitted by a Gaussian. The intensity is in counts per second (counts/s).

shown in the inset of Fig. 1(c). The unit cell is monoclinic, as shown in Fig. 1(a). A more detailed description of the crystal structure can be found in Ref. [14]. The Laue pattern in Fig. 1(c) manifests the twofold symmetry of the crystal structure. In particular, a clear low-energy electron diffraction (LEED) pattern taken after the photoemission measurements demonstrates that the cleaved sample surface is of reasonably high quality [Fig. 1(d)]. As guided by the thin dashed lines there, the symmetry of the triangular lattice is clearly visible here.

The high sample purity and quality can be further illustrated by the x-ray diffraction data of a $EtMe_3Sb[Pd(dmit)_2]_2$ single crystal in Fig. 2(a). The $EtMe_3Sb[Pd(dmit)_2]_2$ single crystal is highly oriented in the **c** direction, since all the peaks could be indexed by (00l). A rocking curve around the (008) peak is shown in Fig. 2(b), which can be well fitted by one Gaussian peak with a resolution-limited full width at half-maximum (FWHM) of 0.06°.

The polarization-dependent ARPES measurements were conducted at Beamline 7U of the Ultraviolet Synchrotron Orbital Radiation Facility (UVSOR). In-house measurements were performed with randomly polarized 21.2-eV He-Iα light from a helium lamp. The overall energy resolution was set to 20 meV or better and the typical angular resolution is 0.5°. Fine single crystals of $EtMe_3Sb[Pd(dmit)_2]_2$, $EtMe_3P[Pd(dmit)_2]_2$, and $Et_2Me_2P[Pd(dmit)_2]_2$ were synthesized by an aerial oxidation method [14], preoriented by Laue diffraction, then cleaved *in situ* and measured under ultrahigh vacuum of 6×10^{-11} mbar. During measurements the temperature was kept at 70 K to avoid the onset of charging at 40 K; radiation damage and aging effects are negligible in the presented data (see Appendix for details).

III. RESULTS AND DISCUSSIONS

The normal-emission spectra from the Γ point of the $EtMe_3Sb[Pd(dmit)_2]_2$ Brillouin zone [Fig. 3(a)] are displayed in Fig. 3(b). In order to make sure all states are detected, various photon polarizations were exploited, including the in-plane (p), perpendicular-to-plane (s), left-handed circular, and right-handed circular polarizations. Here, the "plane" is defined by the incident photon beam direction and the outgoing photoelectron trajectory, so that s and p polarizations are sensitive to only odd and even electron wave functions with respect to this mirror plane [26,27]. We found three broad features within the 1.5-eV binding energy range, and they are most pronounced in the p-polarization data. Moreover, their binding energies are robust against the variation of the photon energy, as illustrated in the inset of Fig. 3(b), which is a manifestation of the 2D character of the system. Figure 3(c) illustrates the photoemission intensity along $(0,-\pi/a)$-$(0,\pi/a)$ after deducting a Shirley background as shown in Fig. 4(a), which shows spectral features with negligible dispersion. Furthermore, as displayed in Fig. 3(d), all the photoemission

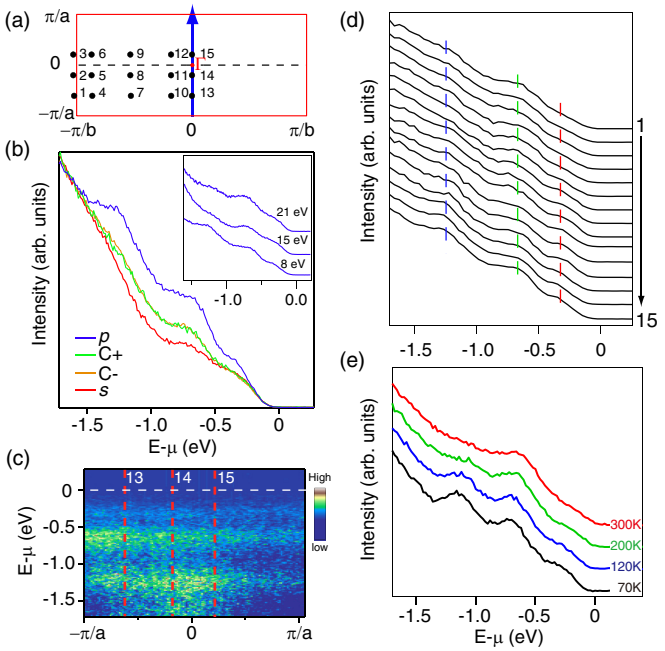

FIG. 3. (Color online) (a) The two-dimensional Brillouin zone of $EtMe_3Sb[Pd(dmit)_2]_2$. (b) The normal-emission photoemission spectra of $EtMe_3Sb[Pd(dmit)_2]_2$ excited by p, s, left-handed circular (C+), and right-handed circular (C−) polarized 8-eV photons. The inset shows the normal-emission spectra collected with p-polarized 8-, 15-, and 21-eV photons. (c) The photoemission intensity along the $(0, -\pi/a)$-$(0,\pi/a)$ line as indicated in (a). (d) ARPES spectra of $EtMe_3Sb[Pd(dmit)_2]_2$ acquired at momenta 1–15 as coded in (a). The photoemission data in (c) and (d) were taken with p-polarized 8-eV photons. (e) Temperature dependence of the normal-emission valence band spectra of $EtMe_3Sb[Pd(dmit)_2]_2$. The data in (e) were acquired with 21.2-eV photons from a helium lamp, and others were collected at UVSOR.

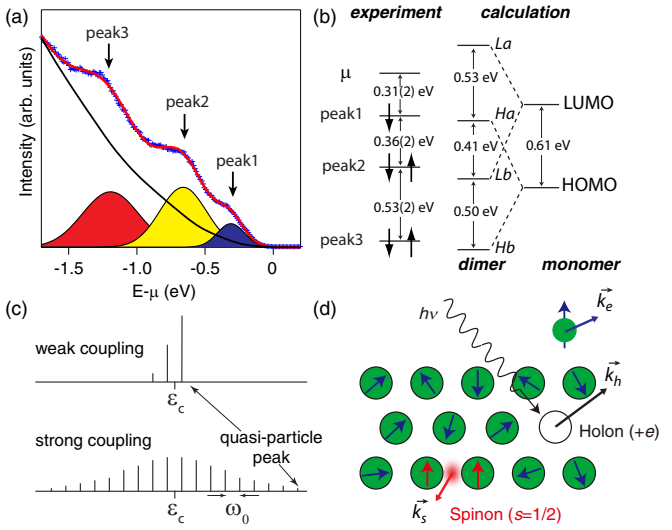

FIG. 4. (Color online) (a) The normal-emission valence-band spectrum of $EtMe_3Sb[Pd(dmit)_2]_2$ is fitted with three Gaussians plus a Shirley-type background. Data were taken with p-polarized 8-eV photons at UVSOR. (b) Left: The centroid of the peaks obtained from the fitting. The black arrows represent the electron spins. Right: The calculated energy levels of the isolated $Pd(dmit)_2$ monomer and $[Pd(dmit)_2]_2$ dimer in $EtMe_3Sb[Pd(dmit)_2]_2$. (c) A schematic spectral function of a single electron coupled to a bath of bosons of frequency ω_0 in the weak- and strong-coupling conditions. (d) Drawing of the spin-charge separation in a QSL, where a photohole splits into spinon and holon excitations.

spectra taken at various momenta in the first Brillouin zone show three specific spectral features, as marked by the dashed lines. However, no obvious momentum dependence of the peak positions is observed, which remarkably contradicts the predicted pronounced dispersions up to 400 meV along $(0, -\pi/a)$-$(0,\pi/a)$ and $(-\pi/b,0)$-$(\pi/b,0)$ [15,16,21]. Figure 3(e) shows the temperature dependence of the normal-emission spectrum. Besides the thermal broadening, no noticeable change is observed, as expected for a QSL.

The normal-emission spectrum of $EtMe_3Sb[Pd(dmit)_2]_2$ is shown in Fig. 4(a), which contains no sharp quasiparticle peaks and can be best fitted with three Gaussian components plus a Shirley-type background for secondary electrons [28]. To compare with the experiment, we have calculated the energy levels of the isolated $Pd(dmit)_2$ monomer and $[Pd(dmit)_2]_2$ dimer in a supercell using their structures in $EtMe_3Sb[Pd(dmit)_2]_2$ with DFT based on the all-electron full-potential linearized augmented plane-wave (FLAPW) method and the QMD-FLAPW12 code [25]. We used the exchange-correlation functional of the generalized gradient approximation (GGA) by Perdew, Burke, and Ernzerhof (PBE) [29]. Muffin-tin sphere radii are set to be 1.06 Å for P, 0.66 Å for C, 1.68 Å for S, and 1.27 Å for Pd. The calculation is only performed at the Γ point with the common size of an orthorhombic lattice of $a = 22.14$ Å, $b = 10.00$ Å, and $c = 13.60$ Å. As illustrated in Fig. 4(b), the interactions between the two $Pd(dmit)_2$ molecules in an isolated dimer will split their respective highest occupied molecular orbital (HOMO) and lowest unoccupied molecular orbital (LUMO) states into bonding and antibonding states, which are labeled as *Hb*, *Ha*, *Lb*, and *La* self-explanatorily. Based on the stoichiometry, there are five electrons, resulting in a half-filled *Ha* band. It is also the fully filled LHB of this Mott insulator. Based on the fitting, the three Gaussian components located at -0.31 ± 0.02, -0.67 ± 0.02, and -1.20 ± 0.02 eV and labeled as peak 1, peak 2, and peak 3 correspond to the *Ha*/LHB, *Lb*, and *Hb* bands, respectively [Fig. 4(b)]. The agreement between the experiment and calculation is reasonably good. Moreover, the spectral weights of peak 2 and peak 3 are comparable, while peak 1 is considerably weaker, which is expected as the LHB is only filled with one electron.

The LHB has no density of state at the chemical potential [Fig. 4(a)], as expected for a Mott insulator. However, its energy gap is rather soft, since the spectral weight gradually increases away from μ, which could be fitted with a power-law relation, as discussed later. U is estimated to be about 0.7 eV for $EtMe_3Sb[Pd(dmit)_2]_2$ [21]. If the upper Hubbard band (UHB) is about 0.7 eV above the LHB located at −0.31 eV [Fig. 4(b)], presumably with similar width, the low-energy tail of the UHB is thus expected to be very close to the chemical potential. This naturally explains the low excitation energy of about 0.04 eV estimated from the resistivity [30]. In other words, our results do suggest that $EtMe_3Sb[Pd(dmit)_2]_2$ is on the verge of a metal-insulator transition, in agreement with the theory [22,23].

The fitted FWHM's of peak 1, peak 2, and peak 3 in Fig. 4(a) are 0.23, 0.40, and 0.48 eV, respectively. The broad line shape that could be fitted with the incoherent Gaussian peaks resembles those of polaronic systems [31–33]. As shown in Fig. 4(c), the quasiparticle weight of a polaronic system is usually vanishingly small at the low-energy edge of the spectrum, and the broad spectrum is an envelope of many individual peaks due to strong electron-boson interactions [34]. For a flexible organic compound with strong spin fluctuations, strong electron-phonon interactions and/or electron-magnon interactions might be expected [35]. Therefore, one might deduce that the charge carriers in QSL could be polarons, which are heavily dressed with phonons and/or magnons. On the other hand, for a polaronic system, it has been shown theoretically that the centroid of the incoherent spectral distribution would follow the bare band dispersion obtained by band calculations [36]. Experimentally, this has been confirmed not only for the systems with strong electron-phonon interactions (e.g., $K_{0.25}Rb_{0.05}MoO_3$) [37] but also for systems with strong electron-magnon interactions, for example, Mott insulators (e.g., NiO, $Ca_2CuO_2Cl_2$) [38,39], and high-temperature superconductors (e.g., $Bi_{1.74}Pb_{0.38}Sr_{1.88}CuO_{6+x}$) [37]. The bare bandwidth of the QSL $Pd(dmit)_2$ salt is as high as 0.4 eV, which should have been readily observed in our experiment if the polaronic scenario had worked.

The dichotomy put forward by the broad linewidth and negligible dispersion might be related to the characteristic electronic properties of a QSL. It is known that the QSL in two dimensions is characterized by deconfined $S = 1/2$ spinons as the fundamental magnetic excitation. Recent torque magnetometry measurements on $EtMe_3Sb[Pd(dmit)_2]_2$ revealed an extended quantum critical phase, in which low-lying gapless spinon excitations behave like the elementary excitations in paramagnetic metals with a Fermi surface [40]. Meanwhile, inelastic neutron scattering of $ZnCu_3(OH)_6Cl_2$, a possible QSL compound on a kagome lattice, shows that its spin excitation is essentially a gapless continuum with very broad momentum distribution over the Brillouin zone [41]. This is very different from the spin waves in usual magnets or the well-defined dispersion of the spinon excitation observed in one-dimensional chains, e.g., $SrCuO_2$ [42]. As demonstrated in Fig. 4(d), if spin-charge separation occurs in $EtMe_3Sb[Pd(dmit)_2]_2$, a photohole would decay into a holon and a spinon [42]. The spinon energy range is small (roughly from zero to J, and J is ~19–22 meV), while the holon dispersion is in the bandwidth scale [42]. Therefore, the spectral function for removing an electron at certain momentum $\vec{k}_e$ would be an entangled function of both spinon and holon excitations summed up over the entire Brillouin zone for both spinon momentum $\vec{k}_s$ and holon momentum $\vec{k}_h$, with the constraint $\vec{k}_e = \vec{k}_s + \vec{k}_h$. In this scenario, since the holons are gapped, we do not observe any Fermi surface for the electron, although the spinon processes a Fermi surface [13]. Moreover, if the spinon is a broad continuum in the energy/momentum phase space for a 2D QSL as suggested by the inelastic neutron scattering, the resulting electron spectral function would lose the momentum information of the holons. Consequently, it naturally explains why the centroid positions of the spectral features match well the energy levels of the isolated dimer, as shown in Fig. 4(b). Furthermore, the spectral

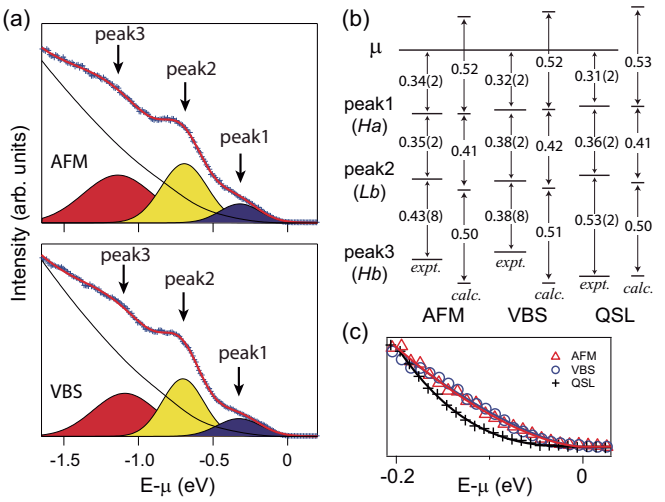

FIG. 5. (Color online) (a) The normal-emission spectra of $Et_2Me_2P[Pd(dmit)_2]_2$ (AFM compound) and $EtMe_3P[Pd(dmit)_2]_2$ (VBS compound) are fitted with three Gaussian peaks plus a Shirley-type background, respectively. Data were taken with p-polarized 8-eV photons at UVSOR. (b) The schematic diagram for the experimental (expt.) and calculated (calc.) energy levels of these materials. The calculated *Ha* bands are individually aligned to the experimental positions of their peak 1's. The unit is electron volts. (c) The Γ-point spectra of the three $Pd(dmit)_2$ salts in the vicinity of the chemical potential, which are fitted to a power-law relation $A \times |E - \mu|^{\alpha}$ (solid lines). The fitted α is 2.8, 1.78, and 1.65 for the QSL, VBS, and AFM compounds, respectively.

width is roughly the same energy scale of the holon bandwidth plus the spinon bandwidth (subjected to the matrix element), in addition to certain scattering effects. Therefore, a possible resolution to the dichotomy is the existence of spin-charge separation in $EtMe_3Sb[Pd(dmit)_2]_2$.

For comparison, the electronic structure of $Et_2Me_2P[Pd(dmit)_2]_2$ (AFM) and $EtMe_3P[Pd(dmit)_2]_2$ (VBS) are investigated at 70 K, so they are not magnetically ordered yet. The ARPES spectra of these compounds show negligible dispersion as well, and the typical spectra are shown in Fig. 5(a). The measured and calculated energy levels of these $Pd(dmit)_2$ salts are presented in Fig. 5(b), which shows reasonable agreement. Near the chemical potential, as shown by the power-law fitting in Fig. 5(c), the gaps for all these compounds are soft ones. For the QSL compound, peak 1 is located at −0.31 eV with a narrower FWHM (0.23 eV) than those of VBS (0.35 eV) and AFM (0.33 eV) compounds, making its spectral weight more suppressed near the chemical potential than the other two. This explains the relatively lower excitation energies of AFM (~26 meV) and VBS (~27 meV) compounds than that of the QSL compound, as estimated from their resistivity data [17,30,43]. Assuming spin-charge separation occurs in these compounds (at least in their magnetic disordered phases studied here), the large widths for the VBS and AFM compounds is consistent with their large hopping integrals [14]. We also note that the variations in the energy-level positions and spectral widths among these $Pd(dmit)_2$ salts in our ARPES data reflect the variations in the

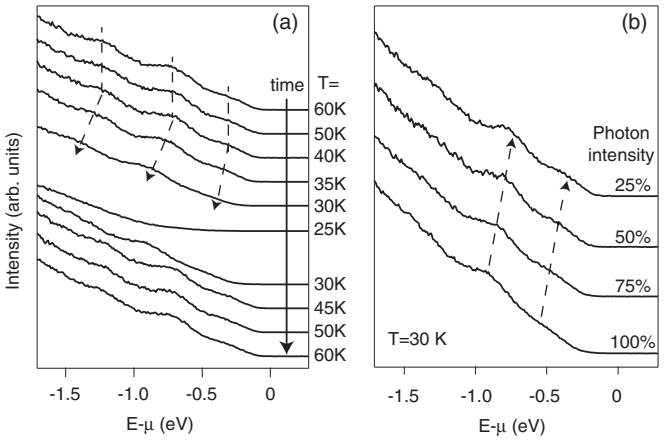

FIG. 6. Photoemission charging effects in $EtMe_3Sb[Pd(dmit)_2]_2$. (a) Temperature dependence of the photoemission energy-distribution curve (EDC) at the Γ point of $EtMe_3Sb[Pd(dmit)_2]_2$. The sample temperature was first lowered, and then raised as indicated. (b) EDC at the Γ point of $EtMe_3Sb[Pd(dmit)_2]_2$ as a function of the photon intensity. Data were taken at 30 K. All the data were collected at UVSOR with *p*-polarized 8-eV photons. Arrows with dashed lines indicate the shift of the features due to the photoemission charging effects.

dimer structure and various energy scales, which would result in different ground states [14].

IV. CONCLUSIONS

To summarize, we have presented the experimental electronic structure of several $Pd(dmit)_2$ salts, showing they are Mott insulators with a soft gap. Moreover, we found that the spectral functions are characterized by negligible momentum dependence and broad line shape, which are rather different from usual polaronlike behavior observed for other antiferromagnetic Mott insulators. We suggest that this could be a direct manifestation of the spin-charge separation in QSL and related compounds. Our results naturally explain many known properties of these materials and would help advancing our understanding of QSL.

ACKNOWLEDGMENTS

We gratefully acknowledge the helpful discussions with Professor D. H. Lee, X. G. Wen, Z. Y. Weng, and F. Wang. This work is supported in part by the National Science Foundation of China, the National Basic Research Program of China (973 Program No. 2012CB921400), and a Grant-in-aid for Scientific Research on Innovative Areas (Grant No. 20110003) from the Ministry of Education, Culture, Sports, Science and Technology (MEXT), Japan.

APPENDIX: CHARGING EFFECT AND RADIATION DAMAGE

In the photoemission study of organic and insulating compounds, it is important to examine the charging effects and radiation damage to the sample.

Figure 6 examines the charging effects in the photoemission process. The temperature dependence of the photoemission spectrum in Fig. 6(a) shows that the three features at −0.31, −0.67, and −1.20 eV of $EtMe_3Sb[Pd(dmit)_2]_2$ move to higher binding energies at 35 K and almost disappear at 25 K. The features reappear upon increasing the temperature. Moreover, if one reduces the intensity of the 8-eV photons at 30 K, these features recover [Fig. 6(b)]. The reactions of these valence-band peaks to the photon intensity and temperature are the typical charging behaviors of an insulator, indicative of a charging effect below 40 K.

Figure 7 checks the radiation damage on $EtMe_3Sb[Pd(dmit)_2]_2$ samples by vacuum ultraviolet (vuv) photons. We found that the distinct features disappear in 0.5 h under high-flux 21-eV photons, as shown in Fig. 7(a). When we lowered the photon energy to 8 eV and reduce the

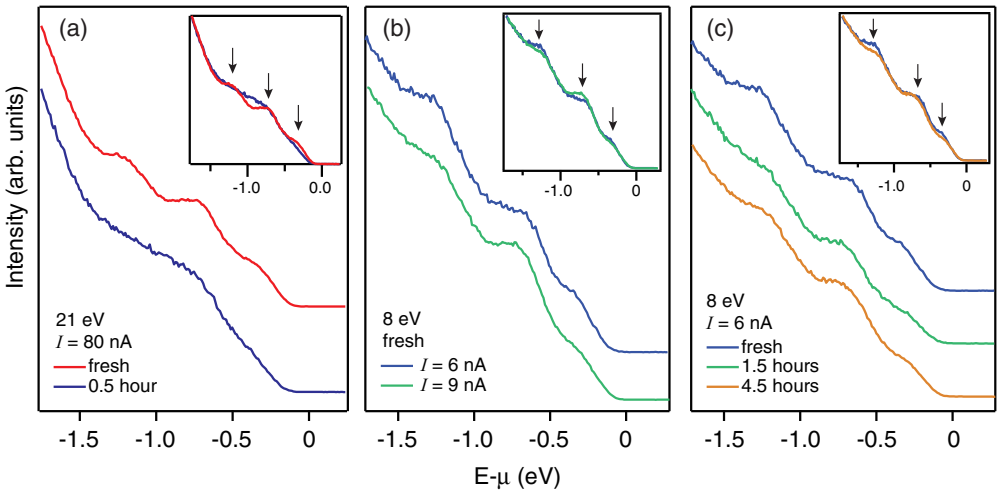

FIG. 7. (Color online) Radiation damage and aging effects in $EtMe_3Sb[Pd(dmit)_2]_2$. (a) EDC at Γ as a function of time with high-flux 21-eV photons. (b) EDC at Γ as a function of photon flux with 8-eV photons. (c) EDC at Γ as a function of time with low-flux 8-eV photons. The photon intensity is measured by a calibrated photodiode, and *I* is its readout photocurrent. All the data were collected at UVSOR with *p*-polarized light. The spectra are overlaid for a better comparison in the insets.

flux, we found that the spectrum was modified only slightly in 4.5 h, as shown in Figs. 7(b) and 7(c), which indicates that the radiation damage and aging effects could be significantly reduced under these experimental conditions.

Based on these studies, we only present fresh ARPES data taken at 70 K and under low photon flux in the main text, so that they are free of charging and aging effects. The observed broad line shape and negligible dispersion are thus intrinsic.

[1] P. A. Lee, N. Nagaosa, and X.-G. Wen, Rev. Mod. Phys. **78**, 17 (2006).

[2] P. W. Anderson, Mater. Res. Bull. **8**, 153 (1973).

[3] Y. Shimizu, K. Miyagawa, K. Kanoda, M. Maesato, and G. Saito, Phys. Rev. Lett. **91**, 107001 (2003).

[4] T. Itou, A. Oyamada, S. Maegawa, M. Tamura, and R. Kato, J. Phys.: Condens. Matter **19**, 145247 (2007).

[5] E. A. Nytko, J. S. Helton, P. Müller, and D. G. Nocera, J. Am. Chem. Soc. **130**, 2922 (2008).

[6] M. P. Shores, E. A. Nytko, B. M. Bartlett, and D. G. Nocera, J. Am. Chem. Soc. **127**, 13462 (2005).

[7] Y. Okamoto, H. Yoshida, and Z. Hiroi, J. Phys. Soc. Jpn. **78**, 033701 (2009).

[8] Y. Zhou, P. A. Lee, T.-K. Ng, and F. C. Zhang, Phys. Rev. Lett. **101**, 197201 (2008).

[9] Z. Hiroi, M. Hanawa, N. Kobayashi, M. Nohara, H. Takagi, Y. Kato, and M. Takigawa, J. Phys. Soc. Jpn. **70**, 3377 (2001).

[10] R. Masutomi, Y. Karaki, and H. Ishimoto, Phys. Rev. Lett. **92**, 025301 (2004).

[11] T. Itou, A. Oyamada, S. Maegawa, and R. Kato, Nat. Phys. **6**, 673 (2010).

[12] T. Itou, A. Oyamada, S. Maegawa, M. Tamura, and R. Kato, Phys. Rev. B **77**, 104413 (2008).

[13] M. Yamashita, N. Nakata, Y. Senshu, M. Nagata, H. M. Yamamoto, R. Kato, T. Shibauchi, and Y. Matsuda, Science **328**, 1246 (2010).

[14] R. Kato and H. Cui, Crystals **2**, 861 (2012).

[15] E. P. Scriven and B. J. Powell, Phys. Rev. Lett. **109**, 097206 (2012).

[16] T. Tsumuraya, H. Seo, M. Tsuchiizu, R. Kato, and T. Miyazaki, J. Phys. Soc. Jpn. **82**, 033709 (2013).

[17] R. Kato, Y. Kashimura, S. Aonuma, N. Hanasaki, and H. Tajima, Solid State Commun. **105**, 561 (1998).

[18] M. Tamura, A. Nakao, and R. Kato, J. Phys. Soc. Jpn. **75**, 093701 (2006).

[19] A. Nakao and R. Kato, J. Phys. Soc. Jpn. **74**, 2754 (2005).

[20] J.-I. Yamaura, A. Nakao, and R. Kato, J. Phys. Soc. Jpn. **73**, 976 (2004).

[21] K. Nakamura, Y. Yoshimoto, and M. Imada, Phys. Rev. B **86**, 205117 (2012).

[22] P. Sahebsara and D. Senechal, Phys. Rev. Lett. **100**, 136402 (2008).

[23] S.-S. Lee and P. A. Lee, Phys. Rev. Lett. **95**, 036403 (2005).

[24] K. Kanoda and R. Kato, Annu. Rev. Condens. Matter Phys. **2**, 167 (2011).

[25] E. Wimmer, H. Krakauer, M. Weinert, and A. J. Freeman, Phys. Rev. B **24**, 864 (1981), and references therein; M. Weinert, E. Wimmer, and A. J. Freeman, *ibid.* **26**, 4571 (1982).

[26] Y. Zhang, F. Chen, C. He, B. Zhou, B. P. Xie, C. Fang, W. F. Tsai, X. H. Chen, H. Hayashi, J. Jiang, H. Iwasawa, K. Shimada, H. Namatame, M. Taniguchi, J. P. Hu, and D. L. Feng, Phys. Rev. B **83**, 054510 (2011).

[27] Y. Zhang, C. He, Z. R. Ye, J. Jiang, F. Chen, M. Xu, Q. Q. Ge, B. P. Xie, J. Wei, M. Aeschlimann, X. Y. Cui, M. Shi, J. P. Hu, and D. L. Feng, Phys. Rev. B **85**, 085121 (2012).

[28] S. Hüfner, *Photoelectron Spectroscopy—Principles and Applications*, Springer Series in Solid-State Science Vol. 82 (Springer, Berlin, 1995).

[29] J. P. Perdew, K. Burke, and M. Ernzerhof, Phys. Rev. Lett. **77**, 3865 (1996).

[30] R. Kato and T. Itou, in *Understanding Quantum Phase Transitions*, edited by L. D. Carr (Taylor and Francis, Boca Raton, FL, 2010).

[31] D. W. Shen, B. P. Xie, J. F. Zhao, L. X. Yang, L. Fang, J. Shi, R. H. He, D. H. Lu, H. H. Wen, and D. L. Feng, Phys. Rev. Lett. **99**, 216404 (2007).

[32] M. Grioni, L. Perfetti, and H. Berger, J. Electron Spectrosc. Relat. Phenom. **137–140**, 417 (2004).

[33] N. Mannella, W. L. Yang, X. J. Zhou, H. Zheng, J. F. Mitchell, J. Zaanen, T. P. Devereaux, N. Nagaosa, Z. Hussain, and Z.-X. Shen, Nature (London) **438**, 474 (2005).

[34] C. Kim, F. Ronning, A. Damascelli, D. L. Feng, Z.-X. Shen, B. O. Wells, Y. J. Kim, R. J. Birgeneau, M. A. Kastner, L. L. Miller, H. Eisaki, and S. Uchida, Phys. Rev. B **65**, 174516 (2002).

[35] H. Tamura, M. Tsukada, H. Ishii, N. Kobayashi, and K. Hirose, Phys. Rev. B **86**, 035208 (2012).

[36] O. Rösch and O. Gunnarsson, Eur. Phys. J. B **43**, 11 (2005).

[37] B. P. Xie, K. Yang, D. W. Shen, J. F. Zhao, H. W. Ou, J. Wei, S. Y. Gu, M. Arita, S. Qiao, H. Namatame, M. Taniguchi, N. Kaneko, H. Eisaki, K. D. Tsuei, C. M. Cheng, I. Vobornik, J. Fujii, G. Rossi, Z. Q. Yang, and D. L. Feng, Phys. Rev. Lett. **98**, 147001 (2007).

[38] F. Ronning, K. M. Shen, N. P. Armitage, A. Damascelli, D. H. Lu, Z.-X. Shen, L. L. Miller, and C. Kim, Phys. Rev. B **71**, 094518 (2005).

[39] Z.-X. Shen, R. S. List, D. S. Dessau, B. O. Wells, O. Jepsen, A. J. Arko, R. Barttlet, C. K. Shih, F. Parmigiani, J. C. Huang, and P. A. P. Lindberg, Phys. Rev. B **44**, 3604 (1991).

[40] D. Watanabe, M. Yamashita, S. Tonegawa, Y. Oshima, H. M. Yamamoto, R. Kato, I. Sheikin, K. Behnia, T. Terashima, S. Uji, T. Shibauchi, and Y. Matsuda, Nat. Commun. **3**, 1090 (2012).

[41] T.-H. Han, J. S. Helton, S. Chu, D. G. Nocera, J. A. Rodriguez-Rivera, C. Broholm, and Y. S. Lee, Nature (London) **492**, 406 (2012).

[42] B. J. Kim, H. Koh, E. Rotenberg, S. J. Oh, H. Eisaki, N. Motoyama, S. Uchida, T. Tohyama, S. Maekawa, Z. X. Shen, and C. Kim, Nat. Phys. **2**, 397 (2006).

[43] R. Kato, A. Tajima, A. Nakao, and M. Tamura, J. Am. Chem. Soc. **128**, 10016 (2006).